#### **Research Article**

Arkadiusz Złocki\*, Maciej Roskosz, Tomasz Krakowski, and Tomasz Mucha

# Analysis of the possibility of applying a residual magnetic field for lack of fusion detection in welded joints of S235JR steel

https://doi.org/10.1515/eng-2025-0119 received January 29, 2025; accepted April 23, 2025

Abstract: The purpose of the conducted research was to verify the possibility of detecting one of the most dangerous defects in welded joints, which are lack of fusion, on the basis of measurements and analysis of residual magnetic field distributions. The radiographic method was used as a reference method, giving a real picture of welding imperfections occurring in the samples. Two types of sensors, a fluxgate sensor and a magnetoimpedance sensor, were used in magnetic field measurements. A calibration procedure was developed and applied for each of them. Residual magnetic field distributions were obtained from the measurement results. Based on these, the distributions of gradients and relative gradients were determined. Comparison of the obtained results with radiographs showed the possibility of detecting a lack of fusion on the basis of magnetic images of welded joints. In addition, the possibility of using both types of magnetic field sensors for magnetic imaging of lack of fusion in welded joints was demonstrated.

**Keywords:** nondestructive testing, welding defects, magnetic memory method, residual magnetic field, magnetic filed sensors, lack of fusion, welded joints

#### 1 Introduction

In order to ensure the reliable operation of structures and machinery, it is crucial to obtain precise information about

\* Corresponding author: Arkadiusz Złocki, Department of Mechanical Engineering and Transport, Faculty of Mechanical Engineering and Robotics, AGH University of Krakow, Al. A. Mickiewicza 30, 30-059, Kraków, Poland, e-mail: zlocki@agh.edu.pl

Maciej Roskosz, Tomasz Krakowski, Tomasz Mucha: Department of Mechanical Engineering and Transport, Faculty of Mechanical Engineering and Robotics, AGH University of Krakow, Al. A. Mickiewicza 30, 30-059, Kraków, Poland

their technical condition. The optimal solution is to obtain this information by non-invasive methods. One of the nondestructive testing methods is the magnetic metal memory (MMM) method, which is gaining popularity [1,2]. This method is based on the use of changes in the electromagnetic properties of materials, resulting from the presence of micro- and macro-scale defects and damage in its structure [3-5]. The basic physical phenomena affecting the electromagnetic properties include the magnetomechanical effect, magnetic field leakage caused by discontinuities or inhomogeneities in the material structure, and processes of interaction of magnetic fields with dislocations and their concentration [6,7]. The method of magnetic memory of metal uses the anomalies of the own residual magnetic field of the test objects, treating the formation of these anomalies as a result of the existence of zones of stress concentration.

One of the potential applications of MMM is the validation of the condition of welded joints, along with the detection of defects inside the welds, because they are potential stress concentrators and therefore magnetic field changes. However, it should be taken into account that not only defects inside the weld can be the causes of field changes. Notch effects or thermal deformation after welding can also be included as causes of stress concentrations [8]. The application of MMM in the test of welded joints is currently being studied in many research centers.

Chen *et al.* [9] studied specimens made of S235 steel. Two blocks of material were welded together intentionally introducing weld defects in the form of cracks and porosity. Subsequently, the presence and location of defects were confirmed by using ultrasonography. Studies of the residual field showed changes in the field values and its gradients at the locations of the previously confirmed defects.

An analysis of the ability to detect slag inclusions and lack of fusion in welded joints was studied by Xing *et al.* [10]. The joints were additionally loaded at 0, 150, and 230 kN, and between the load changes, own residual magnetic field and radiographic tests were performed to determine the presence of defects in the joints and relate them

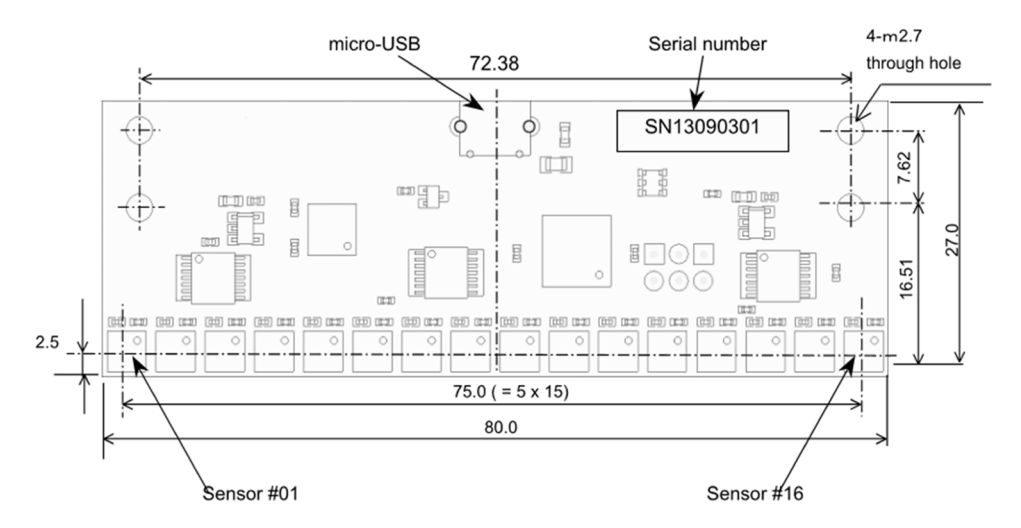


Figure 1: Structure of the sensor AMI 305-16AR [12].

to previous measurements. Changes in MMM signals and gradients were observed in the zones where defects were present. As the load increased for the absence of remelting, the amplitude of the signals increased, while the gradient changed little. For slag inclusions, an increase occurred in signal amplitude and gradient.

Xing *et al.* [11], investigating a pressure vessel that had been heated after welding, showed no changes in magnetic field values and gradients that could indicate defects in the welds. The vessel was then filled with a corrosive medium. The joints were subjected to further tests 6 months and 1 year after filling. Changes in the values and gradients of the magnetic field were shown. Where there was an

increase in gradient values of more than 10 A/m/mm, radiographic examination showed a stress corrosion crack.

The above studies confirm the applicability of MMM using signal analysis and gradients to detect defects in welds. However, the research did not confirm the possibility of determining the type of defect based on the analysis of the aforementioned diagnostic signals.

The purpose of the study was to verify the ability to detect the lack of fusion in welded joints as one of the most dangerous defects in welds. The obtained MMM indications were compared with radiographic results to verify the possibility of detecting a lack of fusion.



Figure 2: Hemholtz coil manufactured by ARM Robotics Sp.z.o.o.

# 2 Research details

# 2.1 Research equipment

Two types of sensors were used: fluxgate and magnetoimpendance. The manufacturer of the TSC-3M-12 measuring

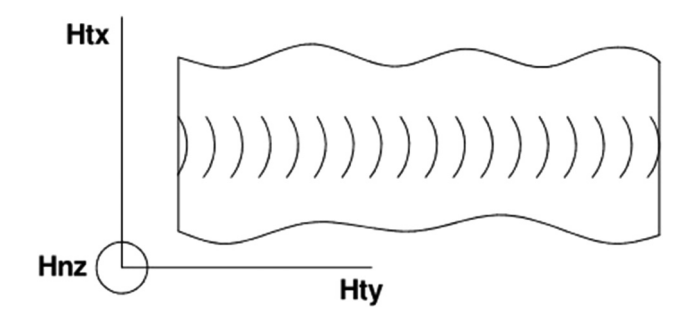


Figure 3: Distribution of magnetic field components.

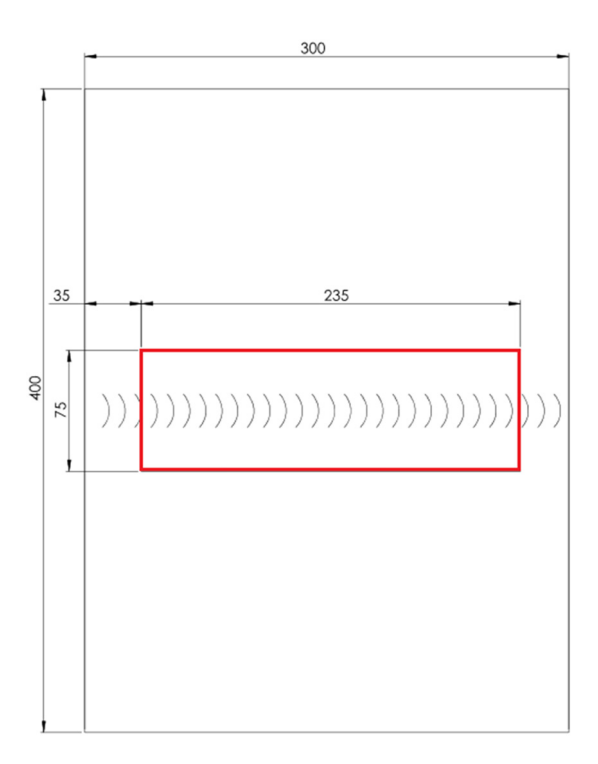


Figure 4: Drawing of the test specimens with the test area marked.

device and the TSC-2M measuring head, which includes two fluxgate sensors, is Energodiagnostika Moscow. The head allows measurement of the three components of the magnetic field by using the core saturation phenomenon and analyzing the second harmonic. The measurement range of the head used is  $\pm 2,000$  A/m with an error of  $\pm 5\%$ . The scanning resolution is 1 mm.

The second AMI 305-AR16 (Figure 1) sensor used was manufactured by Aichi Steel Corporation and consists of 16 AMI 305 triaxial sensors (vector magnetoimpedance magnetometers) with 5 mm spacing using impedance change to measure magnetic field values. The sensor's measurement range is  $\pm 6$  Gauss with a measurement error of  $\pm 0.3$  Gauss. In addition, the measurement system uses an ER40A8192Z5 encoder with a resolution of 8,192 p/r from Eltra Trade and a National Instruments USB-6216 16-channel measurement card with a sampling rate of 400 kS/s along with software developed to record the data obtained.

#### 2.2 Achieve measurement consistency

#### 2.2.1 Calibration procedures

In order to achieve measurement consistency, calibration procedures were carried out for the sensors used. The flux-gate sensor was placed in a Helmholtz coil manufactured by ARM Robotics Sp.z.o.o., (Figure 2) which allows the generation of a magnetic field of a known, constant value. Calibration was performed for a field value of 478 A/m, according to the procedure implemented in the TSC-3M-12 device, thus enabling calibration for three field components.

In order to calibrate the AMI 305-16AR sensor, it was placed in a ZG-212 external magnetic field suppression chamber made of mumetal alloy (an alloy of nickel 75% and iron 15%) with a factory-built demagnetizing coil and a plastic base under the chamber, from manufacturer

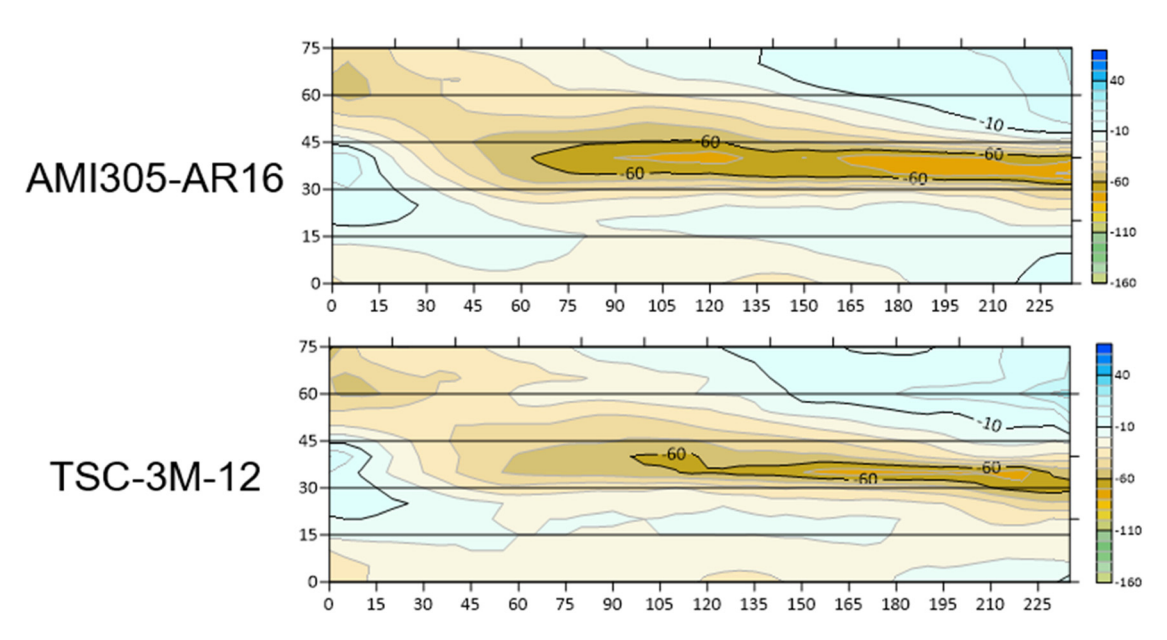
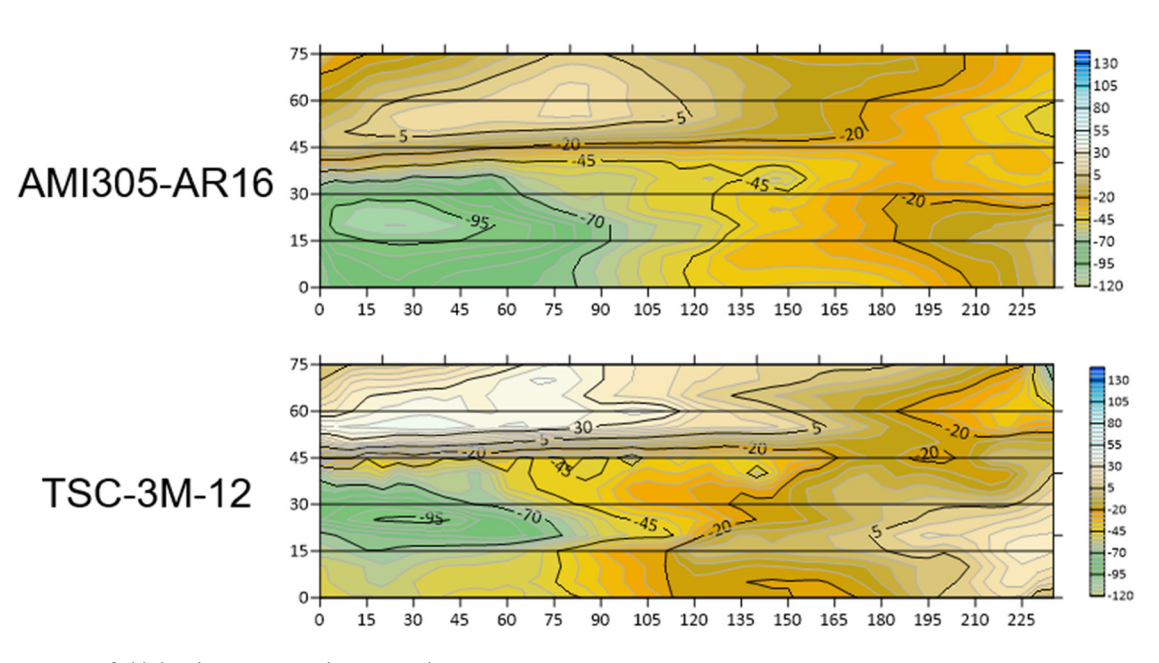


Figure 5: Magnetic field distribution – Sample 1, tangential component, measured in the direction perpendicular to the weld  $H_{t,x}$ .



**Figure 6:** Magnetic field distribution – Sample 4, normal component  $H_{n,z}$ 

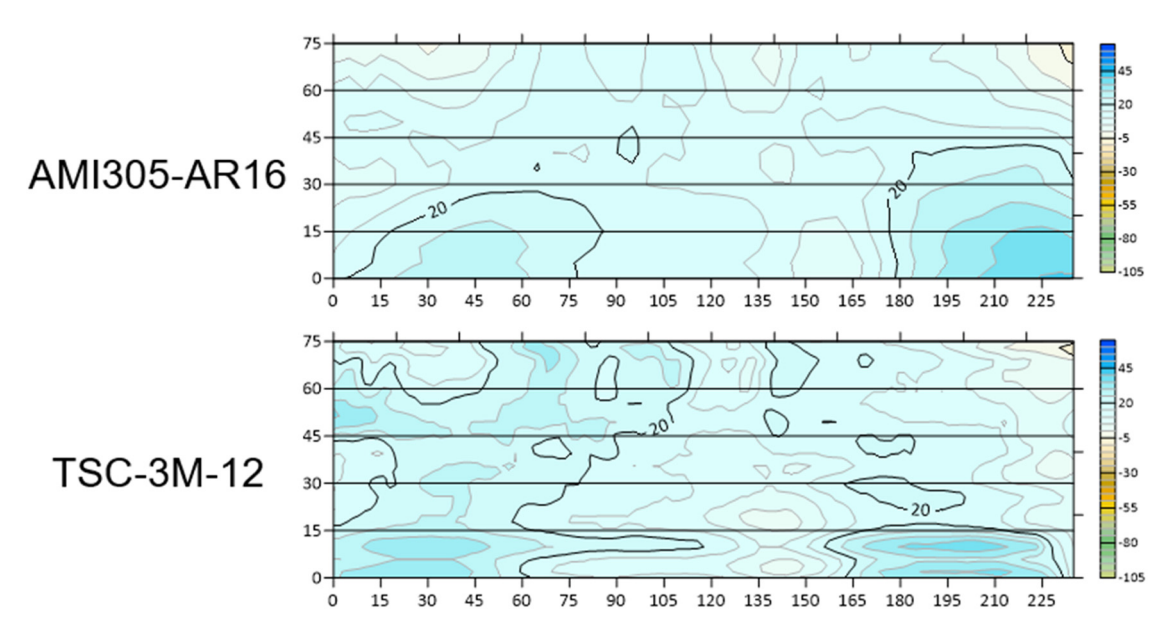


Figure 7: Magnetic field distribution – Sample 2, tangential component, measured in the direction parallel to the weld  $H_{t,v}$ .

Magnetic Shield Corporation (USA). The external magnetic field and the Earth's geomagnetic field (0.25–0.65 Gs) are attenuated to mG levels due to the multi-layer design. Located in the chamber, the sensor is zeroed using control software.

Measurements were made on the surface of the samples from the face and the weld root, making passes parallel and perpendicular to the weld with both sensors (Figure 3); the length of the test section was 235 mm:

•  $H_{t,x}$  – tangential component, measured in the direction perpendicular to the weld,

- $H_{t,y}$  tangential component, measured in the direction parallel to the weld, and
- $H_{n,z}$  normal component.

#### 2.2.2 Description of the specimens tested

Four specimens made of two  $200 \times 300 \times 5$  mm plates connected by a welded joint, made of S235JR steel, were tested. Figure 4 shows a drawing of the tested specimens. Red box marks the measurement area.

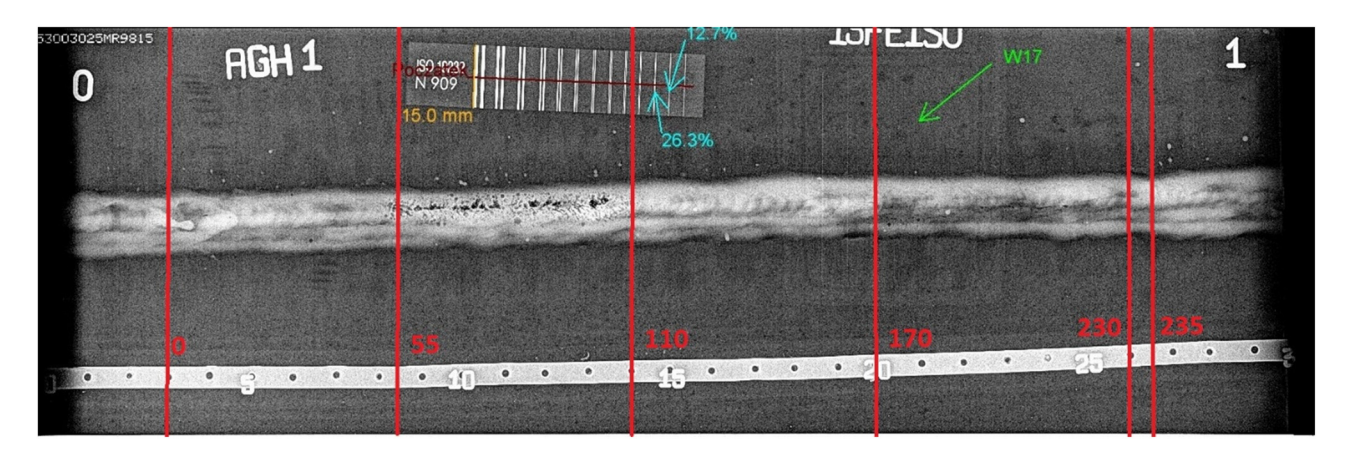


Figure 8: Radiogram of Sample No. 1 with marked test area and location of defects.

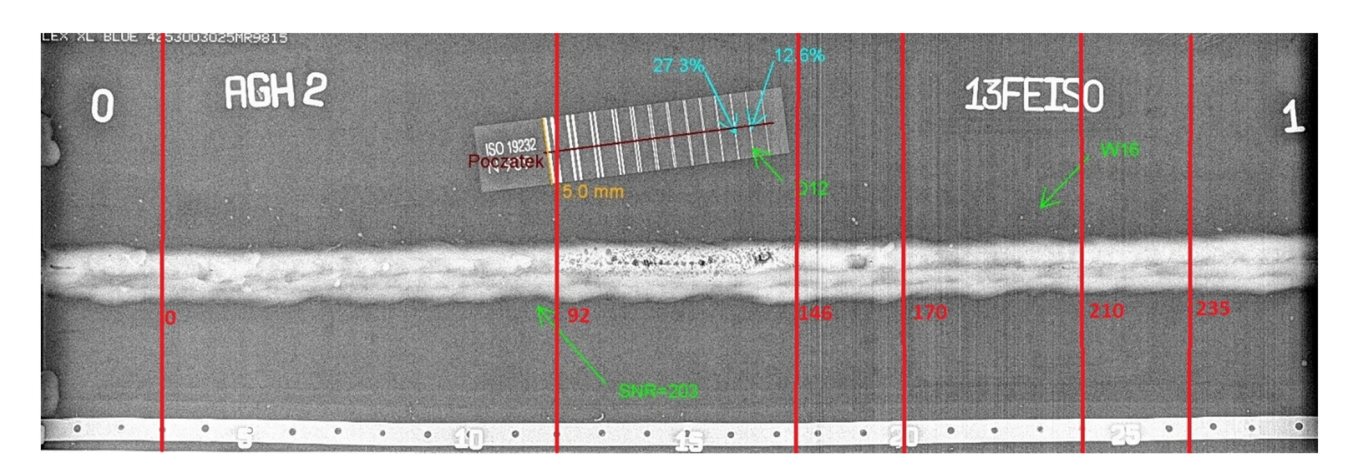


Figure 9: Radiogram of Sample No. 2 with marked test area and location of defects.

#### 2.2.3 Comparison of measurement results

Maps of magnetic field distributions obtained from measurements with both sensors on the tested areas of the samples were prepared and compared. Figure 5 shows the

distributions of the  $H_{t,x}$  component of Sample 1, measured from the weld root for the AMI305-AR16 and TSC-3M-12 sensors. Comparing the obtained distributions, a similarity is evident for both sensors. Measured values are also similar to each other, it should be noted that a weak magnetic field is

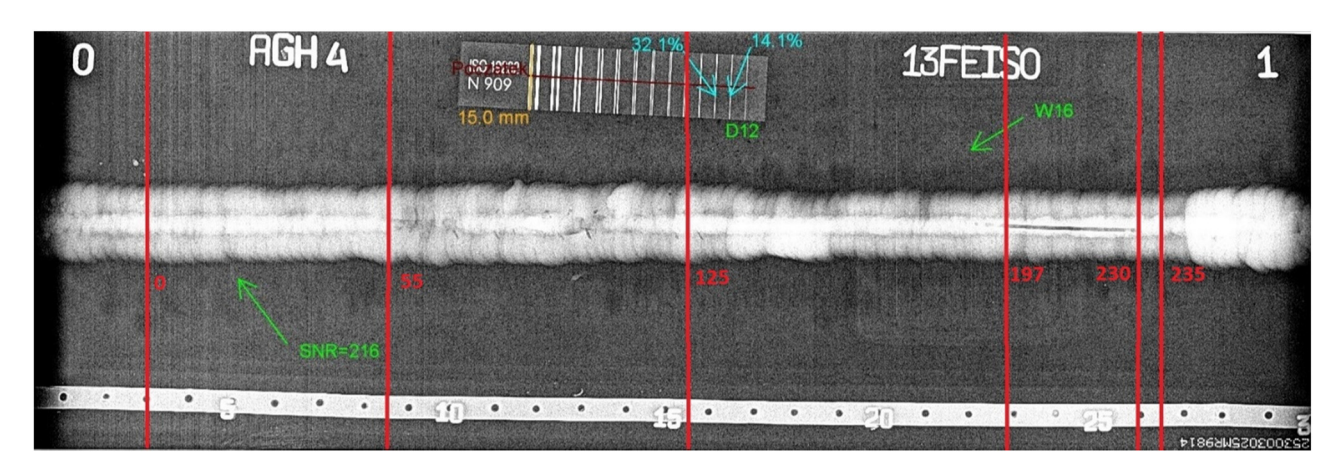
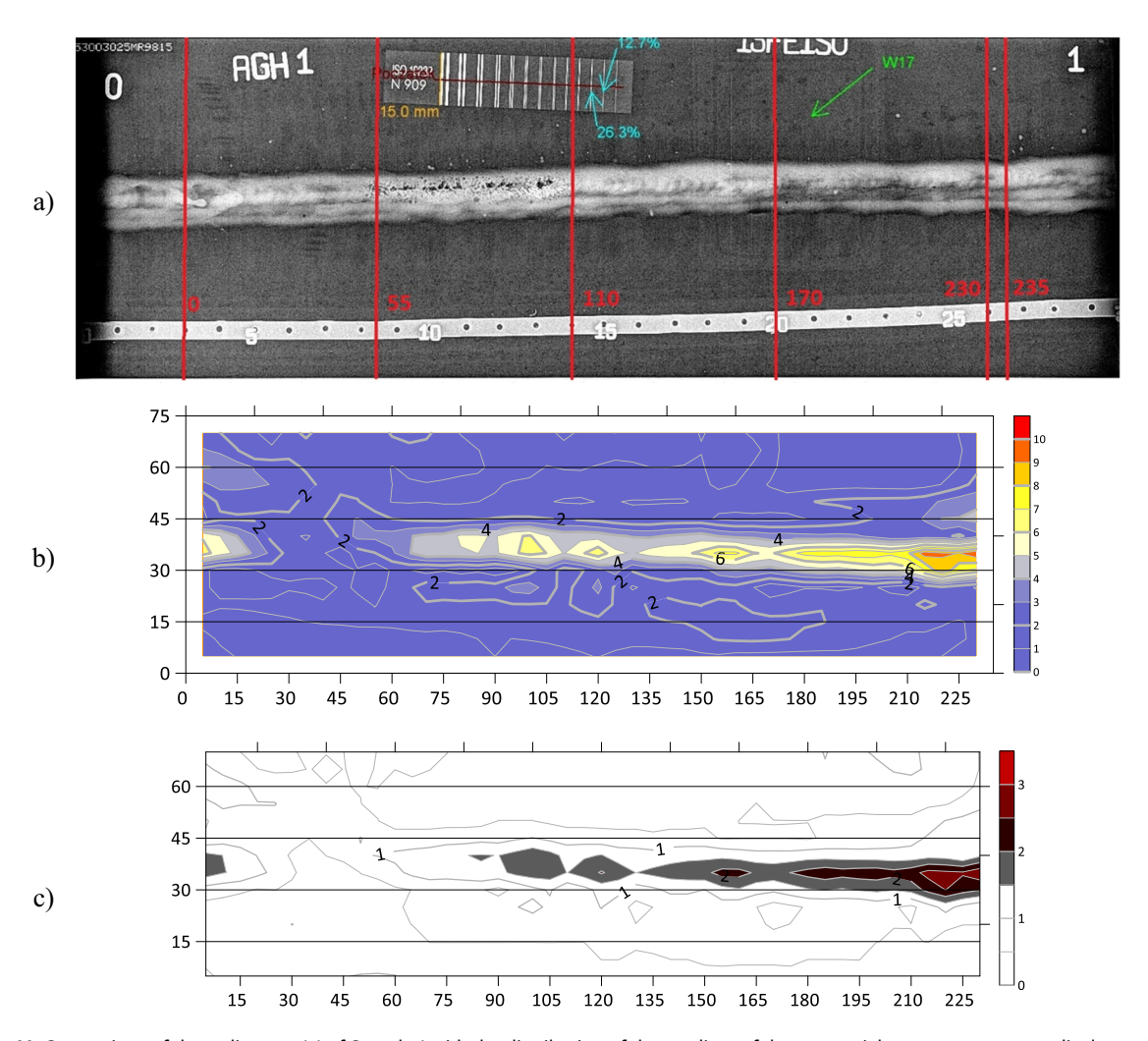


Figure 10: Radiogram of Sample No. 4 with marked test area and location of defects.

6 — Arkadiusz Złocki et al. DE GRUYTER



**Figure 11:** Comparison of the radiogram (a) of Sample 1 with the distribution of the gradient of the tangential component, perpendicular to the weld measured from the face of the grad  $H_{t,x}$  (b) and its magnetic index m- $H_{t,x}$  (c) AMI305-AR16 sensor.

being measured by which the readings may differ to a small extent due to measurement errors of the sensors.

The similarity in the magnetic field distributions is also evident for Sample 4. Figure 6 shows a comparison of the obtained distribution maps of the normal component  $H_{n,z}$  of the magnetic field measured from the weld face.

For Sample 2, the distribution of the tangential component parallel to the weld magnetic field  $H_{t,y}$  is shown in Figure 7. The field values obtained from the two sensors are similar with a very similar distribution.

Analyzing the above distributions and taking into account that the weak magnetic fields were studied and

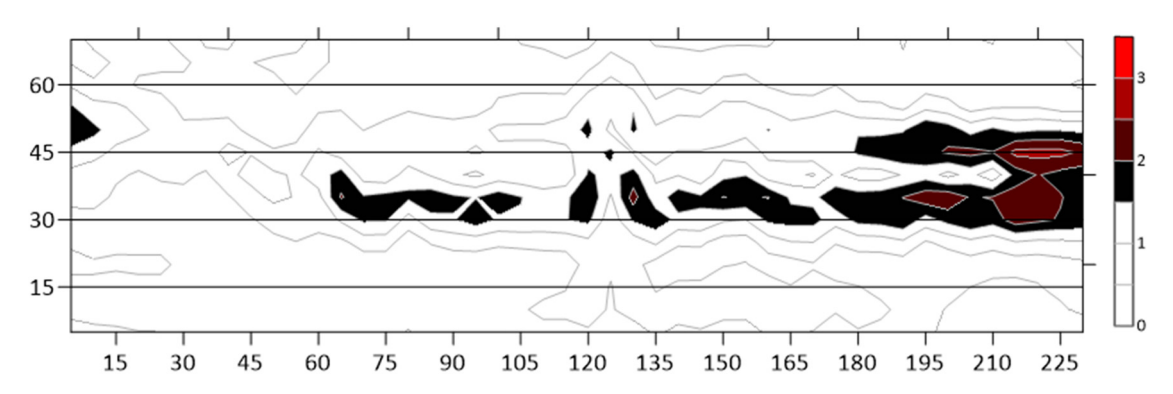


Figure 12: Distribution of the magnetic index of the tangential component perpendicular to the weld m- $H_{t,x}$  Sample 1-TSC-3M-12 sensor.

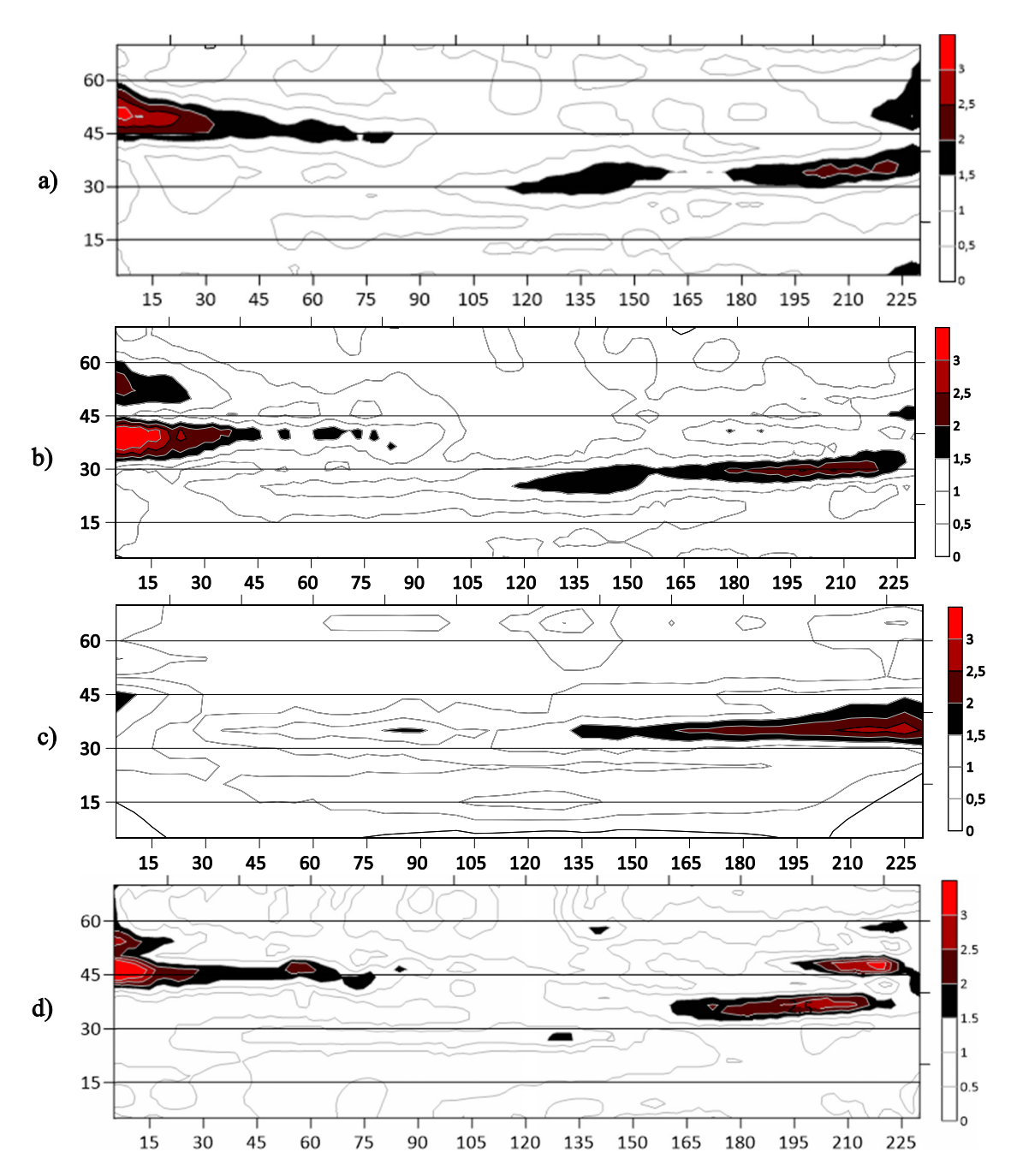


Figure 13: Comparison of magnetic index distributions of Sample 2 components measured from the weld root surface: (a) tangential component, perpendicular to the weld m- $H_{t,x}$  – AMI305-AR16 sensor, (b) normal component m- $H_{n,z}$  – AMI305-AR16 sensor, (c) tangential component, perpendicular to the weld m- $H_{t,x}$  – TSC-3M-12 sensor, (d) normal component m- $H_{n,z}$  – TSC-3M-12 sensor.

the measurement error of the sensors, it can be confirmed that the proposed processes for their calibration ensured the achievement of measurement consistency for both devices. The measurement results are qualitatively and quantitatively consistent and therefore can be used interchangeably in diagnostic work.

## 2.3 Radiographic images

The samples were radiographed using the digital method in accordance with PN-EN ISO 17636-2:2023-04, and their quality was determined in accordance with ISO 19232-1 using the Teledyne ICM/Site-X CP200DS. A current of 8 — Arkadiusz Złocki et al. DE GRUYTER

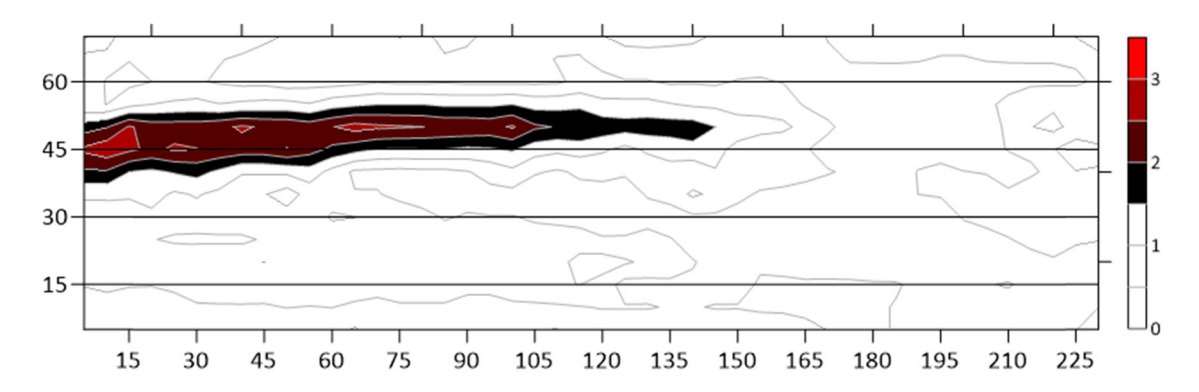


Figure 15: Distribution of magnetic index of Sample 4 normal component m-H<sub>n,z</sub> measured from the weld face with the TSC-3M-12 sensor.

140 kV and 4 mA with an exposure time of 90 s was used. The distance from the test samples was 650 mm. The purpose of the study was to detect and identify defects present in the welds. The radiographs mark the area that was subjected to magnetic testing (0 – beginning of measurement, 235 – end of measurement).

Four specimens were tested, lack of fusion was detected on three; their radiographs are shown in Figure 8. Sample 3, due to the lack of fusion, was neglected.

Figure 8 shows a radiograph of the welded joint of Sample 1, and the presence of pores in the 55–110 area and lack of fusion in the 170–230 area was identified.

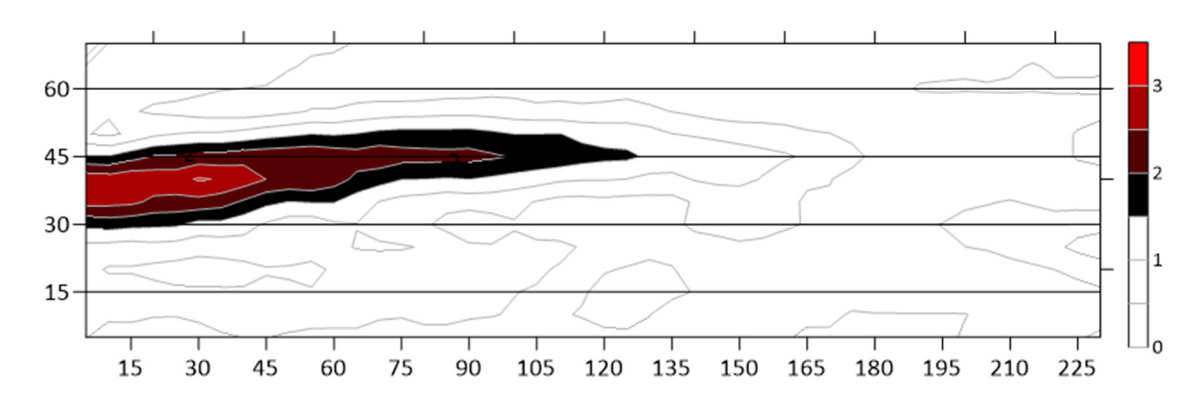
Figure 9 shows a radiograph of the welded joint of Sample No. 2, and the presence of porosity in areas 92–146 and lack of fusion in areas 170–210 was identified.

Figure 10 shows the radiogram of sample 4 with the magnetic test area and the locations of defects marked. For area 55–125, the occurrence of lack of fusion was identified, and for area 197–230, the occurrence of lack of weld penetration was identified.

# 3 Analysis and discussion of the lack of fusion detection capabilities

The results obtained from measurements of the residual magnetic field, made with a fluxgate and magnetoimpedance sensor, on the surface of a welded joint were analyzed to determine the possibility of detecting lack of fusion in welded joints. Changes in the magnetic field on the surface of the test object are usually characterized by a small variation. Areas where this variability is intense are called magnetic anomaly areas and are characterized by higher gradient values. High variability in the value of the measured magnetic field is the result of large changes in the electromagnetic properties of the material under study. This variability can be due to changes at the micro level (changes in the metallographic structure, changes in the residual stresses and their effect on the electromagnetic properties) and changes at the macro level (the occurrence of discontinuities).

By determining the value of the gradient for the individual components of the residual magnetic field, it is possible to identify magnetic anomalies, the cause of which



**Figure 14:** Distribution of magnetic index Sample 4 normal component m- $H_{n,z}$  measured from the weld face with the AMI305-AR16 sensor.

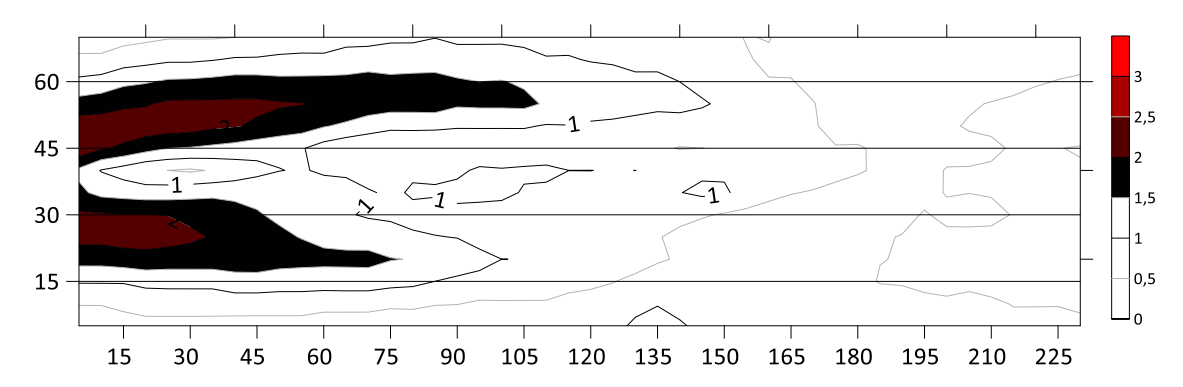


**Figure 16:** Distribution of the magnetic index of the Sample 4 tangential component perpendicular to the weld m- $H_{t,x}$ , measured from the weld face with the AMI305-16AR sensor.

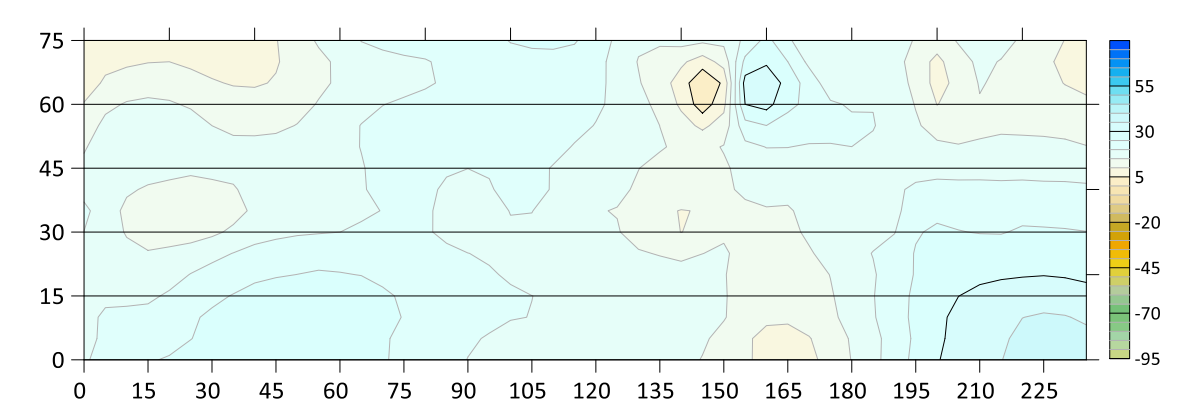


**Figure 17:** Distribution of values of the tangential component parallel to the weld  $H_{t,y}$  of its own residual magnetic field Sample 2 – AMI305-AR16 sensor.

may be areas of stress concentration and thus imperfections in the welded joint. Based on the standard [13–15], the magnetic index m, defined as the ratio of the local gradient value to the average value, was additionally determined.

Figures 11–18 show selected distributions of gradients and magnetic indexes m obtained from the measurement

results, which are representative of the entire study conducted.

For Sample 1 (Figure 11), a correlation can be seen between the radiographic results and the calculated gradient of the tangential component perpendicular to the weld  $grad\ H_{t,x}$  and its magnetic index m- $H_{t,x}$  for the

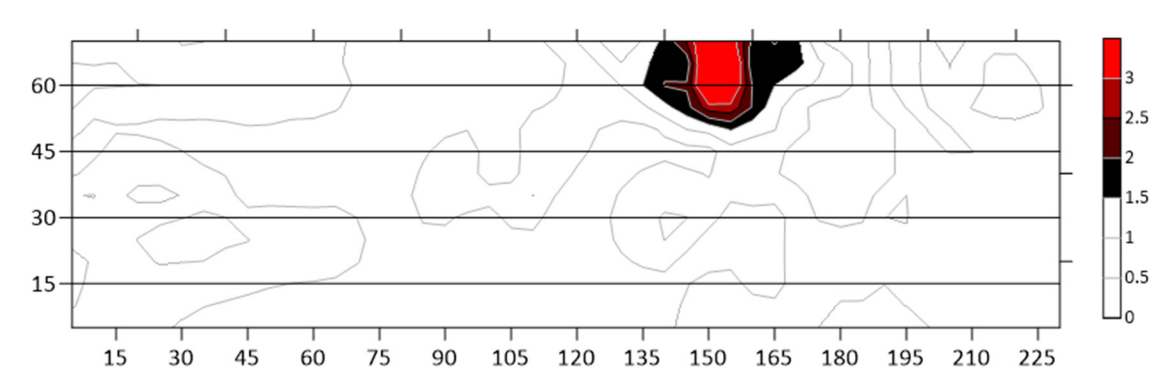


**Figure 18:** Distribution of the magnetic index of the tangential component parallel to the weld m- $H_{t,y}$  of its own magnetic field Sample 2 – AMI305-AR16 sensor.

AMI305-AR16 sensor. There is an increase in the gradient of  $grad\ H_{t,x}$  and the magnetic index  $m\text{-}H_{t,x}$  in the bonding region in the weld (170–230), thus indicating the location of the magnetic anomaly. Comparing the magnetic index  $m\text{-}H_{t,x}$  (Figure 12) calculated for measurements with the TSC-3M-12 sensor with the indication of the radiogram also shows an increase in its value in the area 175–225 (the maximum value in the area is more than 2.5), which coincides with the area of lack of fusion. Changes in the value of the  $m\text{-}H_{t,x}$  index at the edges of the weld are visible, but they are lower than the value of the index in the lack of fusion area. Both sensors used showed a change in the values of the gradient  $grad\ H_{t,x}$  and the magnetic index  $m\text{-}H_{t,x}$ , indicating the occurrence of a magnetic anomaly at the defect site.

Radiogram of Sample 2 (Figure 9) shows the occurrence of a lack of fusion in the 170-210 mm area. On selected magnetic index distributions (Figure 13 (a)  $m-H_{t,x}$ - AMI305-AR16 sensor, (b) m- $H_{n,z}$  - AMI305-AR16 sensor, (c) m- $H_{t,x}$  – TSC-3M-12 sensor, (d) m- $H_{n,z}$  – TSC-3M-12 sensor), it is evident that their values increase in areas partially overlapping with the defect occurrence area. The greatest correspondence between the area of magnetic anomaly occurrence and the defect area has an index distribution for the normal component  $m-H_{n,z}$  measured with both magnetoimpedance and fluxgate sensors (Figure 13 (b) m- $H_{n,z}$  – AMI305-AR16 sensor, (d) m- $H_{n,z}$  – TSC-3M-12 sensor), an increase in the index value of  $m-H_{n,z}$  occurs for the 170–220 mm area. The largest value (more than 3) of the m- $H_{n,z}$  index reaches the 195–210 mm area for the fluxgate sensor. For the index of the tangential component index measured perpendicular to the weld  $m-H_{t,x}$  measured with the AMI305-AR16 sensor (Figure 13a), an increase in value is seen from point 175, but a strong indication (the index exceeds the value of 2) is seen in the 195–225 mm area, overlapping only partially with the lack of fusion area. For the fluxgate sensor, the  $m-H_{t,x}$  index (Figure 13b) increases in value over an area of 160–230 mm, exceeding the defect area on both sides.

For Sample 4, comparing the distributions of the m- $H_{n,z}$  index (Figure 14 [AMI305-AR16 sensor] and Figure 15 [TSC-3M-12 sensor]) with the radiograph (Figure 10), which indicates the occurrence of lack of fusion in the 55–125 mm area, the correlation does not occur, unlike in the other samples. The visible magnetic anomaly begins outside the defined area and only partially overlaps it at the location of the weld edge. For the index of the tangential component perpendicular to the weld m- $H_{t,x}$  for Sample 4 (Figure 16), there were also no visible changes in its value in the defect area, while magnetic anomalies are visible for the weld edges.

The results of the analyzed samples show that for none of them the tangential component parallel to the weld,  $H_{t,v}$ ,

**Table 1:** Summary of the compatibility of the occurrence of magnetic anomalies with the location of the lack of fusion

Sensors Component		AMI305-16AR			TSC-3M-12		
		$H_{t,x}$	$H_{t,y}$	H <sub>n,z</sub>	$H_{t,x}$	$H_{t,y}$	H <sub>n,z</sub>
Sample 1	Face	++	-	++	++	_	++
	Root	++	-	++	+	-	++
Sample 2	Face	+	-	+	+	-	+
	Root	+	-	++	-	-	++
Sample 4	Face	-	-	-	-	_	-
	Root	-	-	-	-	-	-

(-) No compatibility, (+) anomaly partially overlaps, and (++) anomaly overlaps.

did not give satisfactory results. For the specimens studied, the anomalies occurring on it did not coincide with the area of lack of fusion. As an example, the distribution of the value of the tangential component parallel to the weld  $H_{t,y}$  (Figure 17) and the corresponding distribution of the magnetic index m- $H_{t,y}$  (Figure 18) are shown for Sample 2.

# 4 Summary and conclusions

The purpose of the study was to determine the possibility of detecting the lack of fusion in welded joints based on residual magnetic field measurements. It was assumed that two methods of measuring the magnetic signal would be used: fluxgate sensors (TSC-3M-12) and magnetoimpedance sensors (AMI 305-AR16, Aichi Steel). In order to be able to compare the results from the two sensors, it was necessary to achieve measurement consistency by developing calibration procedures for the sensors used. The sensor calibration process developed and carried out made it possible to achieve measurement consistency in a qualitative and quantitative sense for the AMI305-16AR magnetoimpedance sensor and the TSC-3M-12 fluxgate sensor, as demonstrated in the magnetic field distributions shown.

Analysis of the distributions of the gradients of the own residual magnetic field and the magnetic indices makes it possible to determine the location of magnetic anomalies. Comparison of the position of the anomalies with radiographic results (Table 1) showed the possibility of detecting a lack of fusion occurring in welded joints by analyzing the normal component  $H_{n,z}$ , which, according to Table 1, showed the greatest agreement with radiographic results, and the tangential component perpendicular to the weld  $H_{t,x}$ . The configuration of both components allows the detection of a lack of fusion in the welded joint with a

higher probability. Analyzing the appearance of distributions, gradients and indices, it is difficult to identify characteristic features that would allow to distinguish lack of fusion from other welding defects. This issue will be continued in future studies.

**Funding information:** The research was funded by a research subsidy Faculty of Mechanical Engineering and Robotics.

Author contributions: All authors have accepted responsibility for the entire content of this manuscript and consented to its submission to the journal, reviewed all the results, and approved the final version of the manuscript. AZ: data acquisition, methodology, writing, visualization, and interpretation; MR: methodology, conceptualization, writing reviewing and editing, guidance, critical revision, and interpretation; TK: methodology, visualization, validation, and interpretation, TM: methodology and critical revision.

**Conflict of interest:** Authors state no conflict of interest.

Data availability statement: All data generated or analyzed during this study are included in this published article.

## References

Su S, Liu X, Wang W, Li J, Deng IR. A review of metal magnetic memory technology in civil engineering. J Magn Magn Mater. 2024;6:172231. doi: 10.1016/j.jmmm.2024.172231.

- Xu Y. Research progress on magnetic memory nondestructive testing. J Magn Magn Mater. 2023;565:170245. doi: 10.1016/j. jmmm.2022.170245.
- [3] Dubov AA. Development of a metal magnetic memory method. Chem Pet Eng. 2012;47(11-12):837-9. doi: 10.1007/s10556-012-9559-6.
- Bao S, Jin P, Zhao Z, Fu IM. A review of the metal magnetic memory method. J Nondestruct Eval. 2020;39:11. doi: 10.1007/s10921-020-0652-z.
- Deputat J. Principal of the metal magnetic memory method. Dozór [5] Techn. 2002;5:97-105.
- Li L, Jiles DC. Modified law of approach for the magnetomechanical model: application of the rayleigh law to stress. IEEE Trans Magn. 2003;39(5):3037-9. doi: 10.1109/TMAG.2003.815882.
- [7] Jiles D. Theory of the magnetomechanical effect. J Phys D: Appl Phys. 1995;28:1537-46.
- Luming L, Songling H, Xiaofeng W, Keren S, Su W. Magnetic field [8] abnormality caused by welding residual stress. J Magn Magn Mater. 2003;261(3):385-91. doi: 10.1016/S0304-8853(02)01488-9.
- Chen Y, Pan X, Deng L. Study on the localization of defects in typical steel butt welds considering the effect of residual stress. Appl Sci. 2023;13(4):2648. doi: 10.3390/app13042648.
- Xing HY, Zhang LH, Xu C, Chen XY. Welded joint nonpenetration and slag inclusion evaluation based on MMM signal characteristic. AMR. 2011;189:3355-8. doi: 10.4028/www.scientific.net/AMR.189-193.3355.
- Xing HY, Qin P, Lou YM. Design and application of MMM system for [11] welding residual stress test. AMR. 2012;566:534-7. doi: 10.4028/ www.scientific.net/AMR.566.534.
- [12] Aichi Micro Intelligent, "Manual AMI305-16AR". 2013.
- [13] Non-destructive testing metal magnetic memory Part 1: Vocabulary, PN-ISO 24497-1:2009, 2009.
- [14] Non-destructive testing metal magnetic memory Part 2: General Requirements, PN-ISO 24497-2:2008, 2008.
- Non-destructive testing metal magnetic memory Part 3: Inspection of welded joints, PN-ISO 24497-3:2009, 2009.